Transport characteristics of a window-coupled in-plane-gated wire system

Y. Hirayama and Y. Tokura
NTT Basic Research Laboratory, Musashino-Shi, Tokyo 180, Japan

A. D. Wieck, S. Koch,* R. J. Haug, and K. von Klitzing
Max-Planck-Institut für Festkörperforschung, Heisenbergstrasse 1, W-7000 Stuttgart 80, Germany

K. Ploog
Paul-Drude-Institut für Festkörperelektronik, Hausvogteiplatz 5-7, O-1086 Berlin, Germany
(Received 13 April 1993)

Low-temperature ($T \approx 50$ mK) transport characteristics are measured for parallel wires coupled by a ballistic window. The structure is fabricated by focused Ga ion-beam scanning and subsequent annealing. The size of the structure is modified by in-plane-gated operation. At zero magnetic field, the transport characteristics are governed by the mode matching between one-dimensional modes in the wires and quasi-zero-dimensional modes in the window. When four-terminal resistance is measured as a function of in-plane-gate voltage, a small period oscillation is superimposed on the background oscillation corresponding to the subband population in each wire. At intermediate magnetic fields, Aharonov-Bohm interference effects are observed in both the magnetic field and the in-plane-gate voltage dependence. These originate from the circulating channel in the window. Theoretical calculations essentially reproduce the experimental results, supporting these explanations.

I. INTRODUCTION

Electron wave interference plays an important role in the transport characteristics in mesoscopic structures.[1,2] Conductance fluctuations in a wire structure and Aharonov-Bohm (AB) oscillations in a ring structure have been extensively studied. Recently, it has become clear that a wide section or a bending in a wire acts as a cavity and causes many interesting interference effects.[3–13] Many theoretical calculations have been reported for such interference effects. When the size of the cavity is controlled by the gate voltage, the interference pattern is well modified as a function of a gate voltage.[13,14] On the other hand, the coupling between parallel wires is an interesting topic in mesoscopic systems. Coupling through a tunneling barrier or windows has been proposed by analogy to optical and electromagnetic waveguide systems. Some theoretical and experimental results have been reported for the coupling characteristics.[15–19] In particular, wire coupling through a window[18,19] is expected as an efficient coupling system where the electron wave coupling is achieved in a small length scale. However, this type of coupling should include the complicated characteristics peculiar to a bent wire or a narrow-wide-narrow system, and a detailed experimental study has not been carried out for the window-coupled wire system.

Most calculations for these systems have focused on the single-mode region because it has a large signal amplitude and its characteristics are easy to understand. However, a single-mode wire is difficult to achieve with present technology. In particular, a broadening of the corner is inevitable for confinement using depletion region spreading. Therefore the experimental study is limited to the phenomena observed in a multiple-mode system. However, the detailed experiments and their comparison with theoretical calculations are important to understand the basic mechanisms which determine the transport characteristics of a window-coupled wire system. In addition, theoretical calculations are usually carried out as a function of structural size at zero magnetic field ($B=0$ T) in spite of the fact that rich interference effects experimentally appear as a function of a magnetic field. Thus it is interesting to measure the interference characteristics as a function of both size and magnetic field, and to study the interplay between them.

In this study, we fabricated two parallel wires coupled by a ballistic window.[19] This is one of the basic structures for making window-coupled wire systems. It can also be viewed as a narrow-wide-narrow structure where two additional terminals exist at the end of the wide cavity. The position of the depletion boundary defining both the wide cavity region and the terminal wire is modulated by the in-plane-gate operation. Four-terminal resistance representing the coupling between the two wires becomes almost zero over a wide range of in-plane-gate voltage and magnetic field. Therefore, this resistance is sensitive to the electron wave flow in the window region. For example, the ballistic nature of the system causes oscillations corresponding to the subband population of each terminal wire at 1.5 K.[19] When the measurements are carried out below 1 K, the electron wave interference effect dominates the transport characteristics. Large aperiodic and periodic oscillations are observed as a function of in-plane-gate voltage as well as of magnetic field. Although the transport characteristics of a multiple-mode system are complicated and difficult to understand, the in-plane-gate voltage dependence at zero magnetic field and the oscillation as a function of magnetic field observed in an intermediate-field region are well explained

0163-1829/93/48(11)/7991(8)/$06.00

by considering the simple models. These experimental and theoretical results are discussed in this paper.

II. FABRICATION AND MEASUREMENTS

The parallel in-plane-gated (IPG) wires coupled by a small window were formed on an $Al_xGa_{1-x}As$-GaAs modulation-doped heterostructure by focused Ga ion-beam (Ga-FIB) scanning. The initial two-dimensional (2D) electron gas had a carrier density n of 1.6×10^{11} cm^{-2} and a mobility of μ of 5×10^5 $cm^2/V\,s$ at 1.5 K before illumination. A schematic structure of the system is shown in Fig. 1(a), and the central region of the system is enlarged in Fig. 1(b). The Ga-FIB with an acceleration energy of 100 kV and a beam diameter of about $\phi=100$ nm was scanned along the thick solid lines. The interval between the centers of parallel implanted lines is denoted by W, and the length of the unimplanted space along the center line by L. The ion dose was about 10^{12} cm^{-2} and subsequent annealing was carried out at 730 °C to remove implantation-induced damage. Highly resistive regions formed in the Ga-FIB scanned regions remained even after annealing, and depletion spreading from the Ga-FIB scanned lines defined the 2D electron gas.[20] Finally, Au/Ge/Ni ohmic contacts (labeled 1–6) were formed to each 2D electron gas region. Narrow parallel wires were defined between 1 and 2 and between 3 and 4, and they were coupled by a small window at the center. A gate voltage applied to 5 and 6 modulated the depletion region spreading (W_{dep2}) through a lateral field effect (in-plane-gate operation).[21] Thus the effective wire width (W_{eff}) and vertical width of the window ($W_{wind}=2W-2W_{dep2}=2W_{eff}+2W_{dep1}$) could be controlled by gate voltages V_{g5} and V_{g6}. We fabricated two types of structures: a large one with $W=1.25$ μm and $L=1.2$ μm, and a small one with $W=0.65$ μm and $L=0.6$ μm.

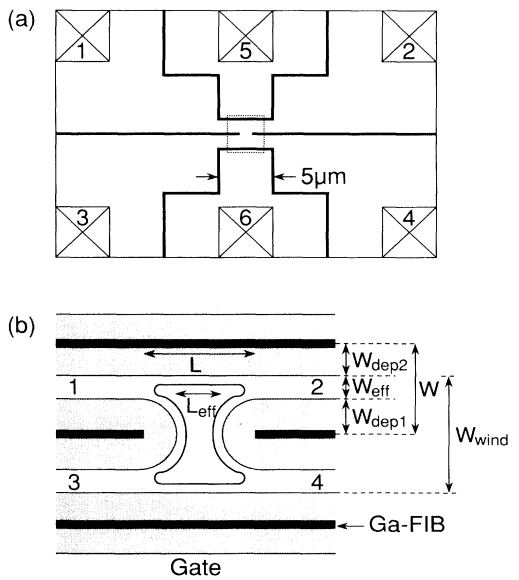

FIG. 1. A schematic diagram of parallel wires coupled by a ballistic window (a). The center region surrounded by the dotted lines is magnified in (b). Black lines indicate Ga-FIB-scanned lines, and ohmic contacts to the 2DEG are indicated by boxed X's and labeled by 1–6. Shadowed regions in (b) represent the depletion region spreading from Ga-implanted lines. In-plane gates (5 and 6) are used to modulate W_{dep2}, and consequently W_{eff}.

Transport characteristics were measured at a lattice temperature of about 50 mK using a dilution refrigerator. The actual electronic temperature might have been somewhat higher due to heating effects, but these would not influence the conclusions of the present work. Three kinds of four-terminal resistance $R_{L1}=R_{12,34}=(V_3-V_4)/I_{1-2}$, $R_{L2}=R_{42,31}$, and $R_H=R_{32,41}$ were measured as a function of magnetic field and in-plane-gate voltage. Here, the same voltage was applied both to 5 and 6 ($V_g=V_{g5}=V_{g6}$). A lock-in technique with a constant ac current of 10 nA was used in this measurement. Reducing the ac current level to 1 nA slightly changed the characteristics in the high-magnetic-field region ($B>5$ T), but not in the low-field region, which includes the complicated fine interference structures. Moreover, the carrier density was gradually increased by repeating a brief illumination at low temperature. The carrier density (n), determined from Shubnikov-De Haas (SdH) oscillations in a high-magnetic-field region, and Fermi energy (E_F) have a simple relation given by $E_F=(h^2/4\pi m^*)n$ for a 2D electron-gas approximation at low temperature, so we indicate E_F in the figures. The depletion spreading decreased with E_F (or carrier density). It was about 500 nm at $E_F=6$ meV ($n=1.8\times10^{11}$ cm^{-2}) and about 250 nm at $E_F=7.7$ meV ($n=2.3\times10^{11}$ cm^{-2}).[19,22] Therefore, the effective wire width W_{eff} of terminal wires was about 250 nm for the large structure when $E_F=6$ meV. For the small system, we need a larger E_F to open the terminal wires. $W_{eff}\approx150$ nm was obtained at $E_F=7.7$ meV. We measured the characteristics when more than five subbands were occupied in each wire, because symmetric ($R_{12,12}\sim R_{34,34}$) and stable characteristics cannot be obtained for a very small wire width. the horizontal window width L_{eff} was estimated from $L-2(W_{dep1}-\phi/2)$, where ϕ is the FIB diameter. Furthermore, the spreading of the depletion region at the edge of Ga-scanned line may be slightly smaller than $W_{dep1}-\phi/2$ due to a reduction in ion dose at the edge. Therefore, $L_{eff}>W_{eff}$ at $V_g=0$ V for both the small and large structures.

III. MAGNETOTRANSPORT CHARACTERISTICS

Transport characteristics were measured as a function of magnetic field at about 50 mK for both the large and small structures. Typical results are shown in Fig. 2 for the large structure, and in Fig. 3 for the small one. The in-plane-gate voltage $V_g=V_{g5}=V_{g6}$ was kept at $V_g=0$ V for both figures. At $B=0$ T, R_{L1} becomes negative, as already observed at 1.5 K, and this negative resistance disappears with increasing magnetic field. This behavior is explained by a sideways ballistic coupling between 1 and 4 (or 2 and 3).[19] This negative resistance is more enhanced for the large structure than for the small one.

Furthermore, fine structures appear at 50 mK, unlike the 1.5-K measurements. The R_{L1} curve in Fig. 2 indicates fine structures in a low-magnetic-field region. Although a variation in background resistance in a low-field region obscures such fine structures in the R_{L2} and R_H curves, these curves contain similarities, as shown below. These fine structures are more enhanced in the small structure, as shown in Fig. 3. Here, the fine structures are clear in every curve (R_{L1}, R_{L2}, and R_H). This is due both to the small window size and the small effective wire width for the small structure under the experimental conditions. In the R_{L1} and R_{L2} curves of Fig. 3, a slowly varying background oscillation, probably corresponding to the SdH oscillations, is visible down to a low magnetic field, and their peak positions agree with the subband depopulation characteristics of each wire.[19] It is noteworthy that fine structures also appear in the quantum Hall regime in Fig. 3. A clear oscillation appears in both R_{L1} and R_{L2} at the higher-field side of the peak between $i=2$ and 4, where i is the filling factor. These oscillations are discussed later in connection with the AB-type interference effects.

Magnetoresistance characteristics in a low-magnetic-field region were studied in detail, and results are shown in Figs. 4 and 5. The in-plane-gate voltage was kept at $V_g=0$ V for these figures. Figure 4 shows characteristics for the large structure, and Fig. 5 for the small structure. Many periodic and aperiodic fine structures appear as a function of magnetic field, and they are completely reproducible as long as the sample is kept at a low temperature. We also measured the characteristics when V_g and/or E_F were varied. The amplitude of fine structures

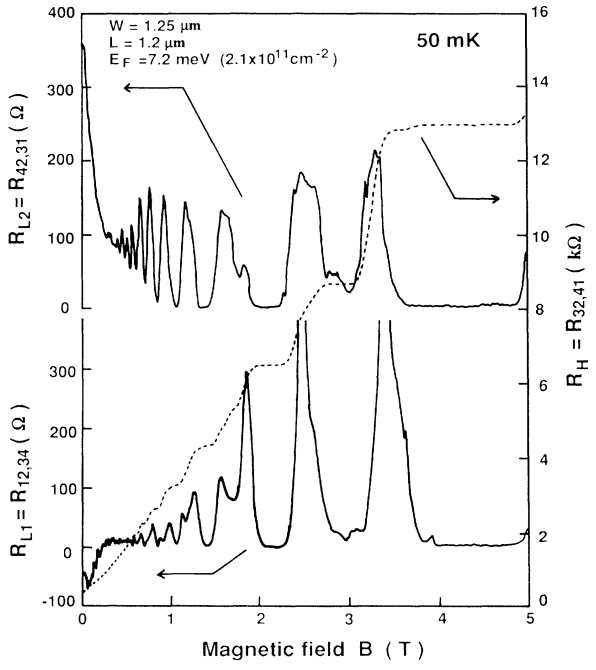

FIG. 2. Four-terminal resistances of the large devices ($W=1.25$ μm and $L=1.2$ μm) measured as a function of magnetic field at 50 mK. $E_F=7.2$ meV and $V_g=0$ V. This condition approximately corresponds to $W_{\text{eff}}\approx 600$ nm. R_{L1}, R_{L2}, and R_H, respectively, correspond to $R_{12,34}$, $R_{42,31}$, and $R_{32,41}$.

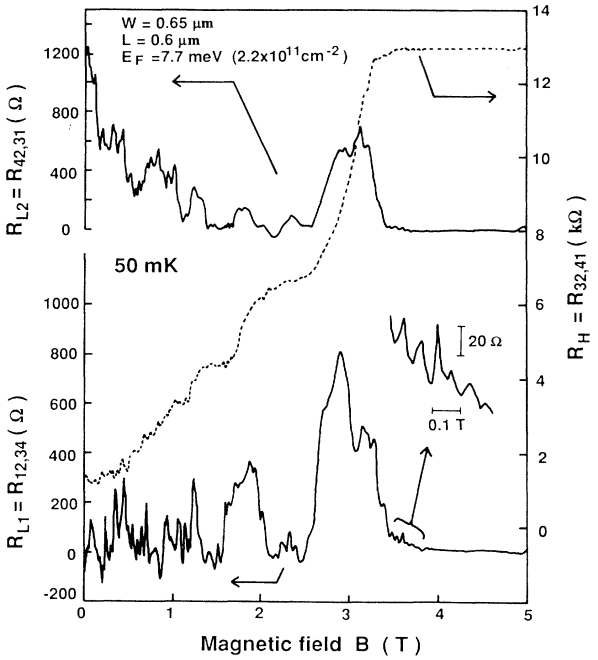

FIG. 3. Four-terminal resistances of the small devices ($W=0.65$ μm and $L=0.6$ μm) measured as a function of magnetic field at 50 mK. $E_F=7.7$ meV and $V_g=0$ V. This condition approximately corresponds to $W_{\text{eff}}\approx 150$ nm.

decreases with E_F (in other words, carrier density) and V_g. This suggests that a narrower W_{eff} is important to obtain distinct fine patterns. In addition, the oscillation period has a tendency to decrease as E_F and V_g increase.

Other interesting features in Fig. 4 are that the oscilla-

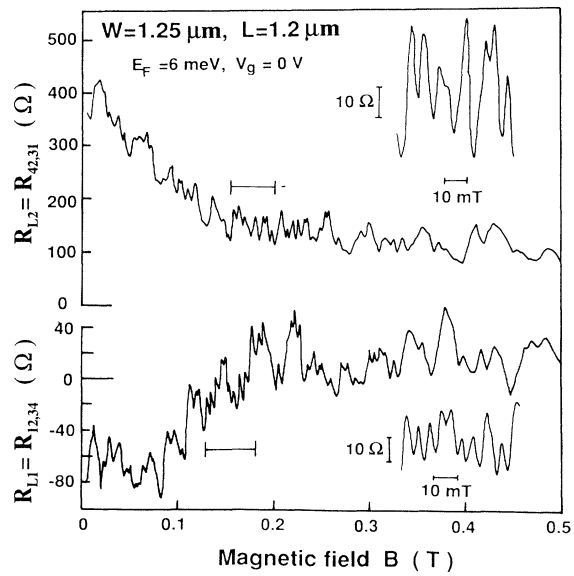

FIG. 4. Detailed traces of $R_{L1}=R_{12,34}$ and $R_{L2}=R_{42,31}$ for the large device measured at 50 mK in a low-magnetic-field region. $E_F=6$ meV and $V_g=0$ V. This value approximately corresponds to $W_{\text{eff}}\approx 250$ nm. Insets show enlarged signals in the field regions indicated by horizontal bars. The slowly varying background is subtracted in these insets.

tion period varies as a function of magnetic field, and that it has a minimum at around $B=0.2$ T, where both the negative R_{L1} and the drastic decrease in R_{L2} disappear. Oscillations in this magnetic-field range are shown enlarged in the insets of Fig. 4. The slowly varying background is subtracted, so that fine oscillation patterns become clear in these insets. The average period is $\Delta B \sim 6$ mT at $E_F=6$ meV. Although the oscillation is less regular with large than with small E_F, the average period decreases with E_F and becomes $\Delta B \sim 4$ mT at $E_F=7.6$ meV. The peak interval increases in the lower-field region. The average period around $B=0$ T is about twice that around $B=0.2$ T. The peak interval also increases in the larger field region ($B \gtrsim 0.3$ T), and fine structures finally disappear leaving SdH oscillation. These characteristics of fine structure are similar in both R_{L1} and R_{L2}. However, the amplitude of fine oscillations is twice as large in R_{L2} than in R_{L1}.

Similar characteristics are reproduced for the small structure (see Fig. 5), except that peak intervals become large and the oscillation amplitude is enhanced. Although the small interval structures are seen in some parts of the R_{L2} curve, the most regular and smallest interval of about $\Delta B=20$ mT is observed at around $B=0.6$ T. That ΔB is four times larger for the small structure than for the large structure suggests an AB-type interference effect. This is because the two-times difference in scale between the two structures makes a four-times difference in the window area. Actually, the area encircled by the sold line in Fig. 1(b) is approximately $S=0.9$ μm^2 for the large structure with $E_F=6$ meV, which agrees with $\Delta B=(h/eS)=4.6$ mT. The negative R_{L1} and the drastic decrease in R_{L2} disappear at the magnetic field, where $r_{cyc}=W_{depl}$, where r_{cyc} is the cyclotron radius. The $W_{depl} \approx 500$ nm for the large structure with $E_F=6$ meV results in $r_{cyc}=W_{depl}=500$ nm at $B=0.14$ T, and the $W_{depl} \approx 250$ nm for the small structure with $E_F=7.7$ meV results in $r_{cyc}=W_{depl}=250$ nm at $B=0.31$ T. Therefore, the magnetic-field range, where approximately regular oscillations and the smallest interval are observed in Figs. 4 and 5, is consistent with the condition $r_{cyc} \lesssim W_{depl}$. When we consider a straight injection from the terminal wire, it is reasonable to assume that the circulating trajectory becomes possible under the condition $r_{cyc} \lesssim W_{depl}$. The edge channel is well established at a high magnetic field. However, the smaller r_{cyc} results in a smaller reflectivity at the boundary between terminal wires and the window, so that the AB-type oscillation corresponding to the window area disappears when the magnetic field is increased further.

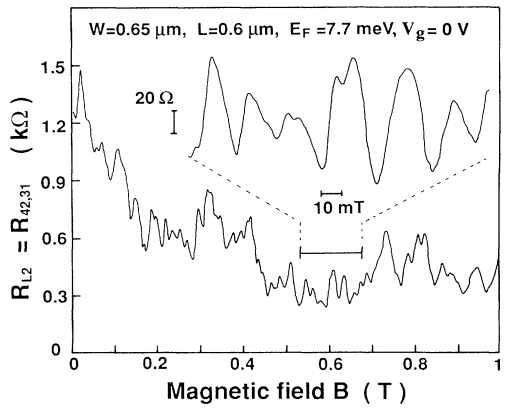

FIG. 5. Detailed traces of $R_{L2}=R_{42,31}$ for the small device measured at 50 mK in a low-magnetic-field region. E_F is 7.7 meV and $V_g=0$ V. This value approximately corresponds to $W_{eff} \approx 150$ nm. Inset shows enlarged signals in the field regions indicted by the horizontal bar. The slowly varying background is subtracted in this inset.

The theoretical calculations were also carried out for a coupled wire system. We calculated R_{L1} and R_{L2} using a recursive Green-function method.[23] We assumed an infinite potential barrier at the boundary and a completely ballistic region inside. For the window geometry, we considered both a rectangular and a rounded shape. The actual experimental setup probably falls between these two shapes. Figure 6 shows the results calculated for the rounded window in a low-magnetic-field region. We set $W_{eff}=260$ nm and $L_{eff}=300$ nm, approximately corresponding to the experiments in Fig. 4. Although $E_F=4$ meV is smaller than the experimental value, the number of subbands (five) in each wire roughly agrees with the experimental conditions where distinct fine oscillations are observed in Figs. 4 and 5. The discrepancy may be explained by the fact that the potential barrier is soft rather than hard in the actual systems.

In spite of the rough approximation in the calculation, the results obtained reproduce the experiments in the following points. (1) The relatively regular, smallest period oscillation exists in the intermediate-field region of 0.1 T $< B < 0.17$ T in Fig. 6. The average period is 5–6 mT, which agrees with the AB-type oscillation corresponding to the window area. (2) The peak interval increases in the lower field region near $B=0$ T. (3) An almost regular but longer period oscillation appears in the higher-field region of $B > 0.17$ T in the R_{L2} curve. On the other hand, the following points are contradictory to the experiments.

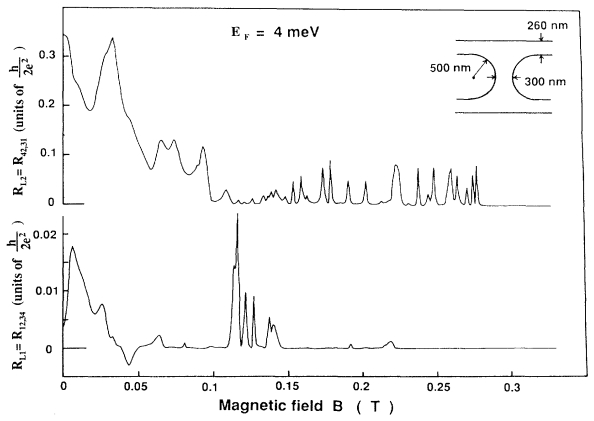

FIG. 6. Theoretical curves of $R_{L1}=R_{12,34}$ and $R_{L2}=R_{42,31}$ as a function of magnetic field. The inset shows the assumed structure with an infinite hard wall. $E_F=4$ meV corresponds to five subbands in each wire as shown in Fig. 8.

(4) The fine patterns are clear in R_{L2} but not in R_{L1}, especially at the field of $B>0.15$ T. (5) The negative R_{L1} at $B=0$ T is not prominent in the calculation. These contradictions probably originate from the imperfectness of the real structure. The ballistic mean free path of electrons is limited by scattering inside the window. In such a case, the shorter length trajectory has a large influence on the resistance. When the ballistic length is comparable to the window size, the direct ballistic coupling between terminals 1 and 4 (or 2 and 3) is still possible through a sideways ballistic component. However, there is no direct coupling between 1 and 3 (or 2 and 4) without boundary reflections. This difference makes $T_{31}T_{42}<T_{32}T_{41}$, thus $R_{L1}=R_{12,34}$ becomes negative as shown in the experimental data. On the other hand, trajectories including many reflections are possible in a completely ballistic system, where the ballistic length is infinite. In this case, long-distance scrambling trajectories make $T_{41}\approx T_{31}$ (or $T_{32}\approx T_{42}$) and result in $R_{L1}=R_{12,34}\approx 0$ as obtained in the theoretical calculation. The difference of fine patterns between R_{L1} and R_{L2} is also explained by the existence of scattering. When we include some imperfection in the calculation, the symmetry of the system is disturbed and the same fine oscillations appear in both R_{L1} and R_{L2}. In this situation, the main characteristics (1)–(3) of the experimental observation are well reproduced in the calculation.

An AB-type oscillation arising from the circulating trajectory in the cavity was reported by van Wees *et al.*[24] in the quantum Hall regime. The coupling between the internal circulating trajectory and the external trajectory by tunneling through a constriction was essential to their experiments. In our experiment, oscillation structures appear in the quantum Hall regime as shown in Fig. 3. The oscillation period is about 50 mT and this value is twice of $\Delta B=20$ mT observed in the low-magnetic-field region (see Fig. 5). This indicates that a half-size window area should contribute to the $\Delta B=50$ mT oscillation. In our system, there was a constriction at the center of the window as well as at the entrance of each terminal wire. Although $L_{\rm eff}>W_{\rm eff}$, the subband depopulation characteristics in the high-magnetic-field region were similar for both terminal wires and the constriction in the window. Therefore, it is possible that the coupling of two trajectories circulating in the upper and lower halves of the window makes the AB-type oscillation similar to that reported by van Wees *et al.*[24]

IV. TRANSPORT CHARACTERISTICS CONTROLLED BY THE IN-PLANE GATE

In this section, we discuss transport characteristics controlled by in-plane-gate operation. The gate voltage $V_g(=V_{g5}=V_{g6})$ applied to both 5 and 6 modulates the depletion spreading $W_{\rm dep2}$ in Fig. 1. The four-terminal resistance $R_{L1}=R_{12,34}$ was measured as a function of V_g at zero magnetic field. The measurements were carried out for the large structure with $E_F=6$ meV. $W_{\rm dep2}\approx W_{\rm dep1}\approx 500$ nm and $W_{\rm eff}\approx 250$ nm at $V_g=0$ V. As shown in Sec. III, R_{L1} is sensitive to the small variation in the transmission probability. The results are shown in Fig. 7. A small period oscillation ($\Delta V_g=0.04$–0.05 V) is superimposed on the background oscillation of $\Delta V_g\approx 0.2$ V. The latter oscillation is also observed at 1.5 K; it is explained by the classical ballistic coupling between two wires through a sideways ballistic component. This coupling is modulated by the subband population in each terminal wire.[19]

A small period oscillation, which is smeared out at 1.5 K, is explained by considering the mode matching between wires and a window. In spite of the existence of open boundaries at the entrances of terminal wires, the formation of quasi-zero-dimensional levels is expected in the window.[3–7,12] First, we roughly assume a convenient structure, a rectangular window ($W_{\rm wind}\times L_{\rm eff}$) with four terminals (width $W_{\rm eff}$). Energy levels perpendicular to the wire are $E_n=\hbar^2/2m^*(\pi n/W_{\rm eff})^2$ (n: integer) in the wire and $E_l=\hbar^2/2m^*(\pi l/W_{\rm wind})^2$ (l: integer) in the window. Energy along the wire is represented as E_F-E_n in the wire and $E_m=\hbar^2/2m^*(\pi m/L_{\rm eff})^2$ (m: integer) in the window. Here, in the window, we neglect open boundaries for terminal wires and this is valid when $W_{\rm eff}\ll W_{\rm wind}$. When the mode-matching condition allows the contribution of the mode with $E_n\approx E_l$ and only the highest subband in the wire contributes to the oscillation characteristics, the relation $E_F-E_n({\rm highest})=E_m$ gives $m=L_{\rm eff}/\pi(2m^*\Delta E/\hbar^2)^{1/2}$ oscillations between subband depopulation. Here, ΔE indicates the energy separation between the highest and the second-highest subband levels in the wire. Substitution of experimental conditions ($L_{\rm eff}\sim 320$ nm, $\Delta E\sim 1.2$ meV) results in 4–5 oscillations between subband populations. In spite of its being a rough approximation, this number agrees fairly well with the experimental observation in Fig. 7. To further confirm the origin of the fine oscillation, theoretical calculation was carried out at $B=0$ T, and results are shown in Fig. 8. The calculation was carried out by dividing the structure into a 20-nm-interval mesh, so that it is difficult to smoothly change the boundary position, i.e.,

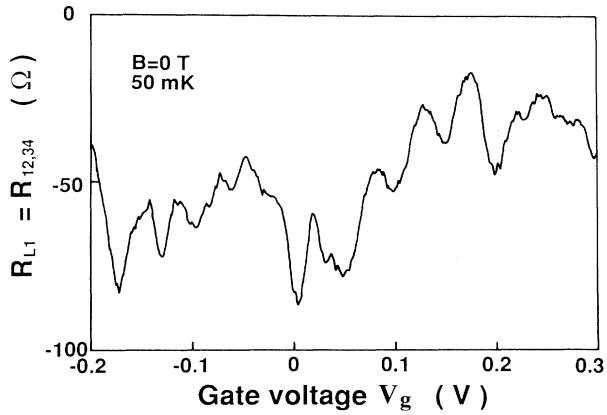

FIG. 7. The four-terminal resistance $R_{L1}=R_{12,34}$ of the large device ($W=1.25$ μm and $L=1.2$ μm) as a function of in-plane gate voltage V_g measured at 50 mK. $E_F=6$ meV and $B=0$ T. A small period oscillation is superimposed on the background oscillation corresponding to the subband population.

the depletion edge of the structure. Therefore, in this calculation, the Fermi energy was varied instead of the in-plane-gate voltage. Fine oscillations superimposed on the background oscillation corresponding to the subband population were reproduced in the calculation. The actual device shape probably falls between the shape of Figs. 8(a) and 8(b). The number of fine oscillations between subband populations is slightly larger than that predicted by a simple mode-matching theory. This is because not only the highest-energy subband but also lower-energy subbands contribute to the calculation. In the experiments of Fig. 7, some fine oscillations are smeared out and the number of fine oscillations between the subband populations becomes smaller than that obtained in Fig. 8. This is again due to the finite ballistic mean free path and finite phase-coherence length in the actual system. In addition, the soft boundary in the real system also induces a suppression of small patterns.

It is noteworthy that the number of oscillations between subband populations is rather insensitive to the boundary shape when the horizontal window width L_{eff} is kept almost constant [see Figs. 8(a) and 8(b)]. On the other hand, this number increases as L_{eff} increases, as shown in Fig. 8(c). The distance between two in-plane gates is kept constant in these three figures. Therefore, these results indicate that fine structures originate not only from electron wave reflection by in-plane gates (a simple Fabry-Perot mode reported by Smith *et al.*[25]) but also from the confinement along the L_{eff} direction. In contrast to experiments by Smith *et al.*,[25] the ratio between W_{eff} and W_{wind} is small in our structure, and quasi-zero-dimensional levels in the window play an important role. These calculated results probably support the mode-matching view for explaining fine resistance oscillation observed at 50 mK.

The four-terminal resistance R_{L1} was also measured as a function of in-plane-gate voltage V_g at $B=0.25$ and 0.4 T. The previously discussed magnetic-field dependence indicated some regular oscillations at around $B=0.25$ T. On the other hand, the fine oscillations became small and SdH oscillation appeared at around $B=0.4$ T. The in-plane-gate voltage dependence is consistent with this magnetic-field dependence. At $B=0.25$ T, a clear oscillation was observed as a function of in-plane-gate voltage V_g, as shown in Fig. 9. The average peak interval is 50 mV, as shown in the inset. Here, we again consider the circulating channel in the window [see Fig. 1(b)]. When in-plane-gate voltage changes W_{dep2}, both the path length l and area S of the circulating channel change. The path

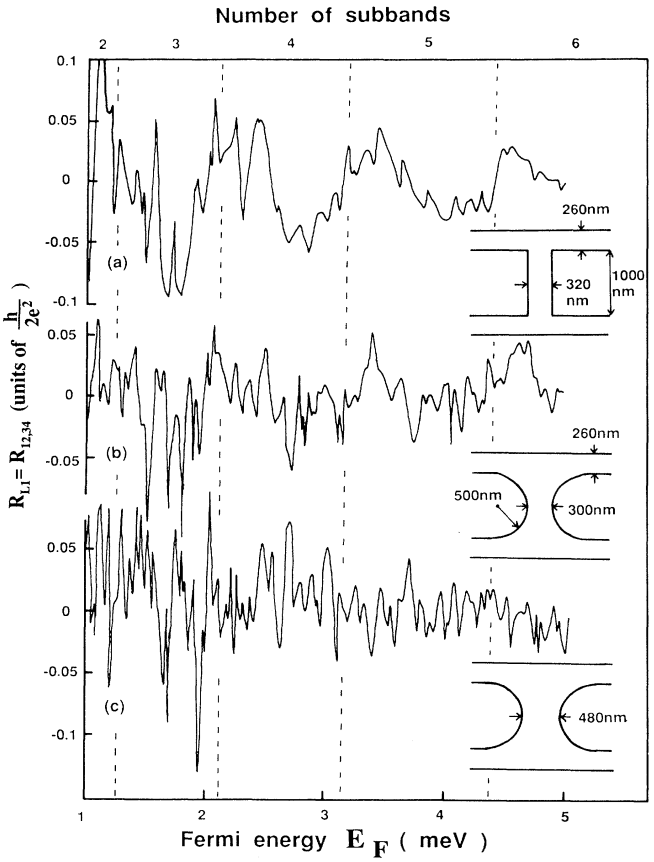

FIG. 8. Theoretical curves of $R_{L1}=R_{12,34}$ as a function of Fermi energy E_F at $B=0$ T. Insets show the assumed structures with an infinite hard wall. The subband population in each terminal wire occurs at E_F indicated by broken lines.

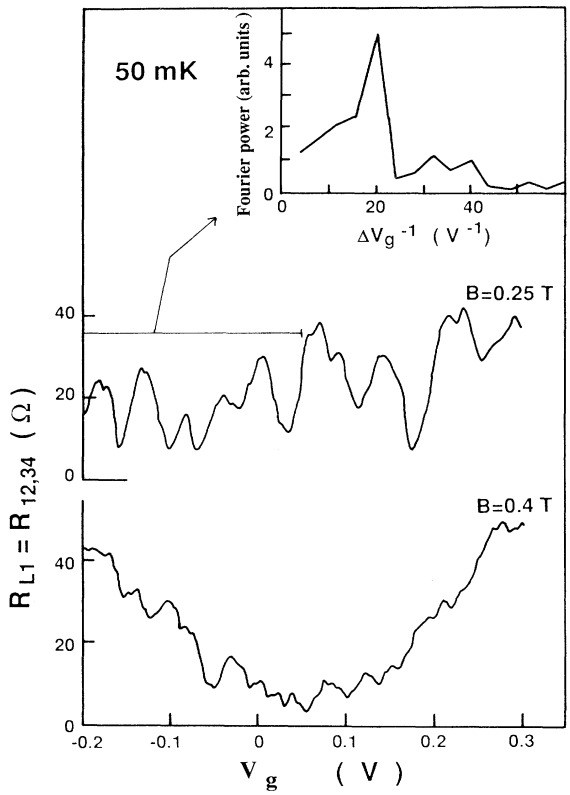

FIG. 9. The four-terminal resistance $R_{L1}=R_{12,34}$ of the large device ($W=1.25$ μm and $L=1.2$ μm) as a function of in-plane gate voltage V_g measured at 50 mK. $E_F=6$ meV and the magnetic fields are $B=0.25$ and 0.4 T. The Fourier spectrum obtained in the V_g region indicated by the horizontal bar is shown in the inset.

length change Δl is approximately four times larger than the change in W_{dep2} ($\Delta l = 4\Delta W_{\text{dep2}}$). As a first approximation, the change in area ΔS is represented as $\Delta S = 2\Delta W_{\text{dep2}} L$. Thus the total change in the AB phase is $k_F \Delta l - (\Delta SBe/\hbar) = (4k_F - 2LBe/\hbar)\Delta W_{\text{dep2}}$. The subband population period of about 0.2 V observed in Fig. 8 and the Fermi wavelength of 60 nm suggest $\Delta W_{\text{dep2}}/\Delta V_g = 300$ nm/V, which agrees well with the data obtained from the conductance characteristics of the single in-plane-gated wires.[22] When we substitute $E_F = 6$ meV, $L = 1.2$ μm, $\Delta W_{\text{dep2}}/\Delta V_g = 300$ nm/V, and $B = 0.25$ T into the above equation, the oscillation period becomes 43 mV. This value almost reproduces the experimental results and confirms that the oscillation as a function of V_g again originates from the AB effect of the circulating channel in the window. At $B = 0.4$ T, the area component becomes large, and the oscillation period should be shorter. Although the oscillatory structures are small and vague, a tendency for short peak intervals is seen in Fig. 9. The slowly varying background observed at $B = 0.4$ T arises from the SdH oscillation. The peak position of the SdH oscillation slowly varies as a function of V_g by the population effect corresponding to W_{eff} and by a slight change of carrier density.

V. SUMMARY

Two parallel in-plane-gated wires coupled by a ballistic window were fabricated by Ga-FIB scanning and subsequent annealing, and transport characteristics were measured as a function of both magnetic field and in-plane-gate voltage at 50 mK. When four-terminal resistance was measured as a function of in-plane-gate voltage at $B = 0$ T, fine oscillatory structures were superimposed on a background oscillation arising from a subband population of terminal wires. Mode matching between one-dimensional levels in the terminal wires and quasi-zero-dimensional levels in the window contributes to the fine structures observed at 50 mK. The agreement between theoretical calculations and experimental results in this study suggests that near-100% current switching between wires will be realized by further reducing a structural size, i.e., the number of modes, as theoretically predicted.[18]

When four-terminal resistance is measured as a function of magnetic field, a small period and rather regular oscillation as a function of magnetic field appears in an intermediate-field region where the negative R_{L1} and the drastic decrease in R_{L2} disappear. The average period is well explained by the AB interference effect through the circulating channel in the window. This interference is also modulated by the in-plane-gate operation. In a higher-magnetic-field region, the peak interval of the fine structure again increases and finally the fine structures disappear leaving the SdH oscillation. However, the interference structures arising from the circulating channel in the window are seen at the foot of the resistance peak in the quantum Hall regime.

ACKNOWLEDGMENTS

We would like to thank T. Bever, T. Ishibashi, and S. Tarucha for their valuable discussions, and A. Fischer and M. Hauser for their expert help with the MBE growth. We are also indebted to Y. Horikoshi and T. Kimura for their encouragement throughout this work. Part of this work was sponsored by the Bundesministerium für Forschung and Technologie of the Federal Republic of Germany.

*Present address: NTT LSI Laboratories, Atsugi-shi, Kanagawa 243-01, Japan.

[1] *Solid State Physics,* edited by H. Ehrenreich and D. Turnbull (Academic, San Diego, 1991), Vol. 44.

[2] *Nanostructure Systems,* Vol. 35 of *Semiconductors and Semimetals,* edited by M. A. Reed (Academic, San Diego, 1992).

[3] Y. Avishai and Y. B. Band, Phys. Rev. B **41**, 3253 (1990).

[4] H. Kasai, K. Mitsutake, and A. Okiji, J. Phys. Soc. Jpn. **60**, 1679 (1991).

[5] T. Itoh, N. Sano, and A. Yoshii, Phys. Rev. B **45**, 14 131 (1992); **47**, 16 601 (1993).

[6] A. Weisshaar, J. Lary, S. M. Goodrick, and V. K. Tripathi, Appl. Phys. Lett. **55**, 2114 (1989).

[7] J. C. Wu, M. N. Wybourne, W. Yindeepol, A. Weisshaar, and S. M. Goodnick, Appl. Phys. Lett. **59**, 102 (1991).

[8] F. Sols and M. Macucci, Phys. Rev. B **41**, 11 887 (1990); C. S. Lent, Appl. Phys. Lett. **56**, 2554 (1990); K. Vacek, H. Kasai, and A. Okiji, J. Phys. Soc. Jpn. **61**, 27 (1992).

[9] C. J. B. Ford, S. Washburn, R. Newbury, C. M. Knoedler, and J. M. Hong, Phys. Rev. B **43**, 7339 (1991).

[10] G. Kirzcenow and E. Castaño, Phys. Rev. B **43**, 7343 (1991).

[11] R. Behringer, G. Timp, H. U. Baranger, and J. E. Cunningham, Phys. Rev. Lett. **66**, 930 (1991).

[12] Y. Takagaki and D. K. Ferry, Phys. Rev. B **44**, 8399 (1991); J. Appl. Phys. **72**, 5001 (1992).

[13] F. Sols, M. Macucci, U. Ravaioli, and K. Hess, Appl. Phys. Lett. **54**, 350 (1989); K. Aihara, M. Yamamoto, and T. Mizutani, Jpn. J. Appl. Phys. **31**, L916 (1992).

[14] R. J. Brown, C. G. Smith, M. Pepper, M. J. Kelly, R. Newbury, H. Ahmed, D. G. Hasko, J. E. F. Frost, D. C. Peacock, D. A. Ritche, and G. A. C. Jones, J. Phys. Condens. Matter **1**, 6291 (1989).

[15] J. A. del Alamo and C. C. Eugster, Appl. Phys. Lett. **56**, 78 (1990).

[16] N. Tsukada, A. D. Wieck, and K. Ploog, Appl. Phys. Lett. **56**, 2527 (1990).

[17] C. C. Eugster and J. A. del Alamo, Phys. Rev. Lett. **67**, 3586 (1991).

[18] J. Wang, Y. J. Wang, and H. Guo, Phys. Rev. B **46**, 2420 (1992); Y. J. Wang, J. Wang, and H. Guo, *ibid.* **47**, 4348 (1993).

[19] Y. Hirayama, A. D. Wieck, T. Bever, K. von Klitzing, and K. Ploog, Phys. Rev. B **46**, 4035 (1992).

[20] Y. Hirayama, T. Saku, and Y. Horikoshi, Phys. Rev. B **39**,

5535 (1989); Y. Hirayama and H. Okamoto, Jpn. J. Appl. Phys. **24**, L965 (1985).
[21]A. D. Wieck and K. Ploog, Appl. Phys. Lett. **56**, 928 (1990).
[22]Y. Hirayama, A. D. Wieck, and K. Ploog, J. Appl. Phys. **72**, 3022 (1992).
[23]T. Ando, Phys. Rev. B **44**, 8017 (1991); Y. Tokura (unpublished).
[24]B. J. van Wees, L. P. Kouwenhoven, C. J. P. M. Harmans, J. G. Williamson, C. E. T. Timmering, M. E. I. Broekaart, C. T. Foxon, and J. J. Harris, Phys. Rev. Lett. **62**, 2523 (1989).
[25]C. G. Smith, M. Pepper, H. Ahmed, J. E. F. Frost, D. G. Hasko, R. Newbury, D. C. Peacock, D. A. Ritchie, and G. A. C. Jones, J. Phys. Condens. Matter **1**, 9035 (1989); C. G. Smith, M. Pepper, H. Ahmed, J. E. F. Frost, D. G. Hasko, D. A. Ritchie, and G. A. C. Jones, Surf. Sci. **228**, 387 (1990).